Effect of secondary radiation force on aggregation between encapsulated microbubbles*

Zhang Yan-Li(张艳丽)[a], Zheng Hai-Rong(郑海荣)[b], Tang Meng-Xing(汤孟兴)[c], and Zhang Dong(章 东)[a]†

[a] *Key Laboratory of Modern Acoustics of Ministry of Education, Institute of Acoustics, Nanjing University, Nanjing* 210093, *China*

[b] *Institute of Biomedical and Health Engineering, Shenzhen Institutes of Advanced Technology, Chinese Academy of Sciences, Shenzhen* 518067, *China*

[c] *Department of Bioengineering, Imperial College London, London, SW7 2AZ, UK*

(Received 8 April 2011; revised manuscript received 5 May 2011)

Secondary radiation force can be an attractive force causing aggregates of encapsulated microbubbles in ultrasonic molecular imaging. The influence of the secondary radiation force on aggregation between two coated bubbles is investigated in this study. Numerical calculations are performed based on four simultaneous differential equations of radial and translational motions. Results show that the secondary force can change from attraction to repulsion during approach, and stable microbubble pairs can be formed in the vicinity of resonant regions; the possibility of microbubble aggregations can be reduced by using low exciting amplitude, ultrasonic frequencies deviating from the resonant frequencies or microbubbles with small compressibility.

Keywords: microbubbles, secondary radiation force, aggregation

PACS: 43.35.Mr, 43.35.Wa **DOI:** 10.1088/1674-1056/20/11/114302

1. Introduction

With the rapid development of targeted microbubbles, ultrasonic molecular imaging has made substantial progress in imaging inflammatory tissue and thrombus, as well as targeting tumor angiogenesis.[1−3] In the targeted imaging system, microbubbles are used as targeted agents, which are expected to adhere to a specific site with a binding mechanism.[4] However, microscopic observations have shown that microbubbles tend to move along the axis of the blood vessel, which leads to low binding efficiency.[5−8] Ultrasound radiation force was proposed as a means to increase the binding efficiency.[9,10] However, these studies are based on the assumption of no interaction between microbubbles, i.e., low concentration of contrast agents is considered. An ultrasonic wave impacts two different types of acoustic radiation forces on the microbubbles. The primary radiation force is generated when the time averaged acoustic pressure around the microbubble has some gradient; while the secondary radiation force is generated between two vibrating microbubbles. Previous studies indicated that the presence of primary radiation force and buoyancy may gather microbubbles in a small region, and provides an opportunity for microbubble aggregation due to secondary radiation force.[11,12] As a result, better understanding of the secondary radiation force is essential for the further development of ultrasonic molecular imaging.

In the study of bubble dynamics, the interaction between bubbles has attracted significant attention both theoretically and experimentally.[13−23] According to the classical Bjerknes theory, if the driving frequency is in between the two resonant frequencies of the individual bubbles, they repel each other; otherwise mutual attraction occurs. However, the discovery of the phenomena of bubble grapes[17,18] and acoustic streamers[19,20] show that real bubbles do not always behave in the aforementioned manner. There seems to be several mechanisms to make bubbles repel each other or form stable bubble pairs with a steady separation. Mettin *et al.* investigated strong sound

*Project supported by the National Basic Research Program of China (Grant No. 2011CB707900), the National Natural Science Foundation of China (Grant Nos. 10974093, 11011130201, and 10904094), the Fundamental Research Funds for the Central Universities of China (Grant Nos. 1103020402, 1116020410, and 1112020401), the Prior Academic Program Development of Jiangsu Higher Education Institutions, China, and the State key Laboratory of Acoustics of Ministry of Education, China.

†Corresponding author. E-mail: dzhang@nju.edu.cn

© 2011 Chinese Physical Society and IOP Publishing Ltd

fields with driving frequency far below the resonant frequencies of two gas bubbles (the driving frequency is 20 kHz).[21] They showed that repulsive interaction forces could be found if the equilibrium bubble radius is a little larger than the dynamical Blake threshold, and that the changeover of the force is caused by a resonance like response of bubbles. Doinikov[22] developed another theoretical model, in which both radial and translational motions of two interacting bubbles are considered. It has been shown that for most combinations of bubble radii, driven well below resonance, mutual attraction leads to a dynamic steady separation between the bubbles rather than collision and coalescence. Both models are confined to the fields of acoustic cavitation and multi-bubble sonoluminescence, where kHz ultrasound is used to excite uncoated air bubbles.

In the application of ultrasound molecular imaging, gas-encapsulated microbubble may exhibit different dynamics from gas bubble owing to the effect of both of its shell and the gas core. The purpose of this study is to find the effect of secondary radiation force on the microbubble aggregation. To achieve this purpose, we studied both the radial and the translational motions of two interacting encapsulated bubbles, and found that the conditions for the attractive mutual forces occur. we also investigated the influence of applied ultrasonic parameters, and shell parameters on microbubble aggregation.

2. Theoretical model

Figure 1 shows two coated microbubbles with equilibrium radii R_{10} and R_{20} in an incompressible viscous liquid. Considering the compressibility of the gas inside the microbubbles, both microbubbles undergo radial and translational oscillations by an ultrasonic wave. Let $R_1(t)$ and $R_2(t)$ denote the time-dependent microbubble radii, and $D(t)$ the time-dependent distance between the microbubble centres. Local axisymmetric spherical coordinates originated at and translated with the centres of the microbubbles are used. In the previous study,[22] Doinikov proposed a theoretical model that makes it possible to calculate radial and translational motions of two interacting spherical gas bubbles in a strong acoustic field. The following four combined ordinary differential equations of second order were used:

$$R_1\ddot{R}_1 + \frac{3}{2}\dot{R}_1^2 - \frac{p_1}{\rho} = \frac{\dot{x}_1^2}{4} - \frac{R_2^2\ddot{R}_2 + 2R_2\dot{R}_2^2}{D} + \frac{R_2^2(\dot{x}_1\dot{R}_2 + R_2\ddot{x}_2 + 5\dot{R}_2\dot{x}_2)}{2D^2} - \frac{R_2^3\dot{x}_2(\dot{x}_1 + 2\dot{x}_2)}{2D^3}, \tag{1}$$

$$R_2\ddot{R}_2 + \frac{3}{2}\dot{R}_2^2 - \frac{p_2}{\rho} = \frac{\dot{x}_2^2}{4} - \frac{R_1^2\ddot{R}_1 + 2R_1\dot{R}_1^2}{D} - \frac{R_1^2(\dot{x}_2\dot{R}_1 + R_1\ddot{x}_1 + 5\dot{R}_1\dot{x}_1)}{2D^2} - \frac{R_1^3\dot{x}_1(\dot{x}_2 + 2\dot{x}_1)}{2D^3}, \tag{2}$$

$$\frac{R_1\ddot{x}_1}{3} + \dot{R}_1\dot{x}_1 + \frac{1}{D^2}\frac{\mathrm{d}}{\mathrm{d}t}(R_1R_2^2\dot{R}_2) - \frac{R_2^2(R_1R_2\ddot{x}_2 + R_2\dot{R}_1\dot{x}_2 + 5R_1\dot{R}_2\dot{x}_2)}{D^3} = \frac{F_{\mathrm{ex1}}}{2\pi\rho R_1^2}, \tag{3}$$

$$\frac{R_2\ddot{x}_2}{3} + \dot{R}_2\dot{x}_2 - \frac{1}{D^2}\frac{\mathrm{d}}{\mathrm{d}t}(R_2R_1^2\dot{R}_1) - \frac{R_1^2(R_1R_2\ddot{x}_1 + R_1\dot{R}_2\dot{x}_1 + 5R_2\dot{R}_1\dot{x}_1)}{D^3} = \frac{F_{\mathrm{ex2}}}{2\pi\rho R_2^2}. \tag{4}$$

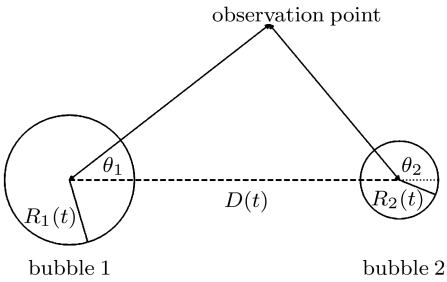


Fig. 1. Schematic diagram of two pulsating and translating microbubbles.

Equations (1) and (2) govern radial pulsations of the bubbles, and Eqs. (3) and (4) describe their translations. Here, $R_j(t)$ and $x_j(t)$ denote the time-varying radius and position of the centre of the jth ($j = 1, 2$) bubble, respectively, p_j is the scattered pressure at the surface of the jth bubble, $F_{\mathrm{ex}j}$ is an external force on the jth bubble such as viscous drag, taken in the form[23]

$$F_{\mathrm{ex}j} = -12\pi\mu R_j(\dot{x}_j - v_{3-j}), \tag{5}$$

where μ is the viscosity of the liquid, the overdot denotes the time derivative, and

$$v_j = (-1)^{j+1}R_j^2\dot{R}_j/(D^2) + R_j^3\dot{x}_j/(D^3). \tag{6}$$

Considering the effect of the shell on the dynamics of encapsulated microbubbles, we replace the well-known Rayleigh–Plesset equation on the left hand side of Eqs. (1) and (2) with the modified Herring equation[10]

$$R_1\ddot{R}_1 + \frac{3}{2}\dot{R}_1^2 - \frac{1}{\rho}\left(P_1 + \frac{R_1}{c}\dot{P}_1 - P_0 - P_{\mathrm{driv}}\right)$$

$$= \frac{\dot{x}_1^2}{4} - \frac{R_2^2\ddot{R}_2 + 2R_2\dot{R}_2^2}{D} + \frac{R_2^2\left(\dot{x}_1\dot{R}_2 + R_2\ddot{x}_2 + 5\dot{R}_2\dot{x}_2\right)}{2D^2} - \frac{R_2^3\dot{x}_2\left(\dot{x}_1 + 2\dot{x}_2\right)}{2D^3}, \quad (7)$$

$$R_2\ddot{R}_2 + \frac{3}{2}\dot{R}_2^2 - \frac{1}{\rho}\left(P_2 + \frac{R_2}{c}\dot{P}_2 - P_0 - P_{\rm driv}\right) = \frac{\dot{x}_2^2}{4} - \frac{R_1^2\ddot{R}_1 + 2R_1\dot{R}_1^2}{D} - \frac{R_1^2\left(\dot{x}_2\dot{R}_1 + R_1\ddot{x}_1 + 5\dot{R}_1\dot{x}_1\right)}{2D^2} - \frac{R_1^3\dot{x}_1\left(\dot{x}_2 + 2\dot{x}_1\right)}{2D^3}, \quad (8)$$

where $P_{\rm driv}(t) = -P_a \sin(2\pi f t)$ is the driving acoustic pressure field, and P_j is the pressure in the liquid at the microbubble wall expressed as

$$P_j = \left(P_0 + \frac{2\sigma_0}{R_0}\right)\left(\frac{R_0}{R_j}\right)^{3\gamma} - \frac{4\mu\dot{R}_j}{R_j} - \frac{2\sigma_0}{R_j} - 4\chi\left(\frac{1}{R_0} - \frac{1}{R_j}\right) - 12\mu_{\rm s}\varepsilon\frac{\dot{R}_j}{R_j\left(R_j - \varepsilon\right)}, \quad (9)$$

where γ is the polytrophic gas exponent. Two additional terms are included. The first term introduces an effective surface tension of the shell following the model proposed by Marmottant *et al.*[24] The variable surface tension $\sigma(R) \simeq \sigma_0 + 2\chi(R/R_0 - 1)$ at elastic state, where σ_0 is the equilibrium surface tension, and χ is the elastic modulus of the shell. The second is a damping term due to the viscosity of the shell, which is given by $12\mu_{\rm s}\varepsilon\dot{R}/(R(R-\varepsilon))$,[24] where $\mu_{\rm s}$ is the viscosity of the shell material and ε is the shell thickness.

3. Results and discussion

In this study, two microbubbles (radius ranges from 0.8 μm to 10 μm) are located with a separation distance D_0. Both have the same microbubble parameters as follows: $P_0 = 1.01 \times 10^5$ Pa, $\rho = 998$ kg/m^3, $c = 1500$ m/s, $\sigma_0 = 0.051$ N/m, $\gamma = 1.07$, $\mu = 0.001$ Pa·s, $\chi \leq 1$ N/m, $\mu_{\rm s} = 1.27$ Pa·s, $\varepsilon = 2\times10^{-9}$ m. Equations (3)–(9) are numerically solved with initial values $R_1 = R_{10}$, $R_2 = R_{20}$, $x_1 = 0$, $x_2 = D_0$ and $R_1' = R_2' = x_1' = x_2' = 0$ at $t = 0$.

3.1. Interaction between two microbubbles

With regard to an encapsulated microbubble, its resonant frequency is derived from the modified Hering equation

$$f_0 = \frac{1}{2\pi r}\sqrt{\frac{1}{\rho}\left(3\gamma P_0 + \frac{4\chi}{r}\right)}. \quad (10)$$

The secondary radiation force coefficient $f_{\rm B}$ is used to determine the dynamic behaviour of two microbubbles, which is defined as[21]

$$f_{\rm B} = \frac{\rho}{4\pi}\left\langle \dot{V}_1\dot{V}_2 \right\rangle, \quad (11)$$

where V_j denotes the volume of the jth microbubble. The sign of $f_{\rm B}$ indicates attraction ($f_{\rm B} > 0$) or repulsion ($f_{\rm B} < 0$) of the microbubbles. Numerical calculations were carried out with driving acoustic pressure amplitude $P_{\rm a} = 0.1$ MPa, and frequency $f = 2.25$ MHz for various initial inter-bubble distances D_0. The resonance radius corresponding to the driving frequency of microbubbles is approximately 2.9 μm according to Eq. (10).

Figure 2 presents the secondary radiation force coefficients in a grayscale mode in the R_{10}–R_{20} plane for two cases $D_0 = 50$ μm and 120 μm. It is found that there exist two distinct dynamical regimes: the white areas indicate repulsion, and dark regions attraction. The repulsive region contains microbubbles with one smaller that and the other larger than the resonant size. While the attractive forces prevail as microbubbles both have radii larger or smaller than the resonance radius. The interaction reaches the peak value (corresponding to the darkest scale) for microbubbles with resonance radii. As the separation distance D_0 decreases, the repulsive regions become a little larger. For example, for a fixed $R_{20} = 7$ μm, in the case of $D_0 = 120$ μm, $R_{10} \leq 3$ μm corresponds to the repulsive region, while $R_{10} \leq 3.05$ μm corresponds to the repulsive region as D_0 is reduced to 50 μm. This demonstrates an inversion of the interaction force as the separation distance decreases and the possibility of the formation of stable microbubble pairs when one bubble is close to the resonance size. The results are qualitatively consistent with that of free bubbles under conditions near the Blake threshold,[21] at which a sign inversion was discovered in the mutual interaction force of two bubbles as the separated distance decreases.

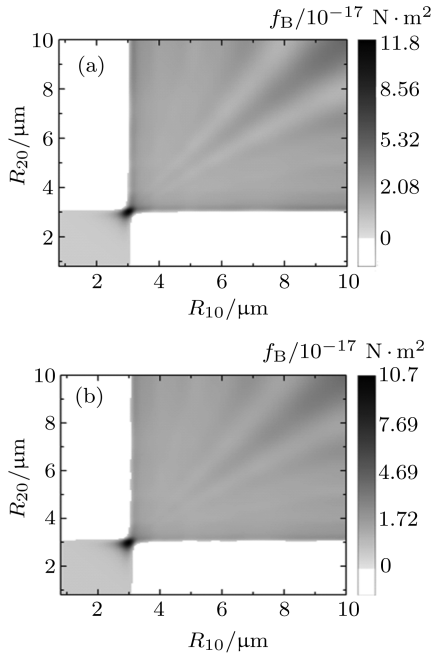


Fig. 2. Dynamic behaviour of two microbubbles driven by a 2.25 MHz acoustic wave. The separated distance is set to be (a) 120 μm, and (b) 50 μm.

Figure 3 shows the change of the secondary radiation force coefficient f_B as the initial separation distance D_0 increases from 30 μm to 120 μm for a selected microbubble pair ($R_{10} = 3$ μm, and $R_{20} = 6$ μm) at 0.1 MPa and 2.25 MHz. As can be seen, the secondary radiation force could change from positive to negative with the decrease of D_0. For example, in the case of $D_0 = 120$ μm, a positive f_B leads to microbubbles attracting each other corresponding to the dark region in Fig. 2(a); as the microbubbles approach a separation distance $D_0 = 50$ μm, the negative f_B produced repulsive microbubbles corresponding to the white region in Fig. 2(b). This shows that the interaction force can change from attraction to repulsion as the microbubbles approach each other.

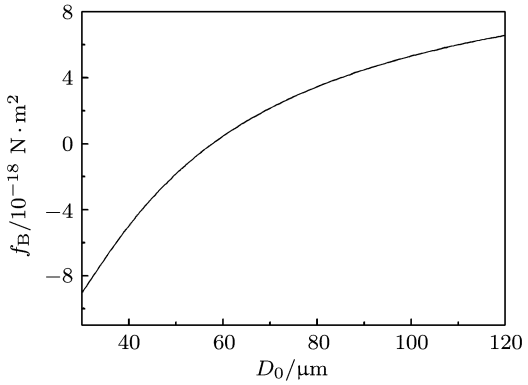


Fig. 3. Change of secondary radiation force coefficient f_B with initial distance D_0 at 0.1 MPa and 2.25 MHz for the bubble pair $R_{10} = 3$ μm, and $R_{20} = 6$ μm.

The formation of a stable microbubble pair is another important aspect of the dynamic behaviour of the two microbubble system. Figure 4 shows the evolution of the averaged separation distance between the two microbubbles in two situations: 1) two microbubbles ($R_{10} = 4$ μm and $R_{20} = 6$ μm) attracted each other until a stable microbubble pair was formed (Fig. 4(a)); 2) two microbubbles ($R_{10} = 3$ μm and $R_{20} = 6$ μm) repelled each other until a stable pair was formed (Fig. 4(b)). It should be noted that in Fig. 4(b), it took about 25 μm to produce a candidate pair, which is much longer than that in Fig. 4(a) (about 0.4 μm). Accordingly, with the increase of time, the slower moving microbubble pair can become a candidate for the formation of stable pairs. Finally, the two pairs of interacting bubbles moved along the same direction with the same translational velocity.

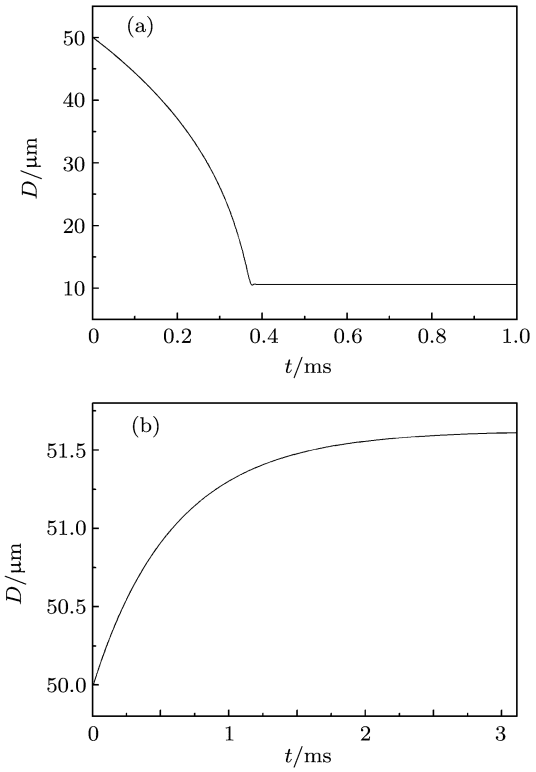


Fig. 4. Evolution of the average distance between the centres of the two microbubbles with elapsed time for (a) $R_{10} = 4$ μm and $R_{20} = 6$ μm, (b) $R_{10} = 3$ μm and $R_{20} = 6$ μm; $D_0 = 50$ μm.

3.2. Effect of acoustic and shell parameters on aggregation

For most ultrasound contrast agents, most microbubbles have a size distribution in the range of from 0.8 μm to 3 μm in radius. For such microbubbles, the secondary radiation force appears as an attractive force as shown in Fig. 2, which leads to an aggregation of microbubbles. This indication is also consistent with previous experimental observations.[12] In

this study, we made a quantitative investigation of the influence of several factors on microbubble aggregation, including acoustic and shell parameters.

Assume that the microbubbles were driven by a 2.25 MHz sinusoidal ultrasound with the pressure amplitude of 0.1 MPa. For simplicity, the radius of the second microbubble was fixed to be $R_{20} = 1.5$ μm, while the radius of the first microbubble was varied. Figure 5 presents the secondary radiation force coefficient $f_{\rm B}$ as a function of R_{10}, where the separation distance D_0 were set to be 30, 40 and 50 μm. It is found that $f_{\rm B}$ exhibits a significant increase when R_{10} approaches its resonance size at about 2.9 μm. Note that there is a sign inversion of $f_{\rm B}$ at $R_{10} = 3.1$ μm as a result of the resonance. For the case of $R_{10} < 3.1$ μm, positive value of $f_{\rm B}$ represents attracting region; while as $R_{10} > 3.1$ μm, microbubbles shows the repulsive behaviour. Additionally, the secondary radiation force increases as the separation distance decreases, indicating that a short separation distance leads to a faster microbubble attraction.

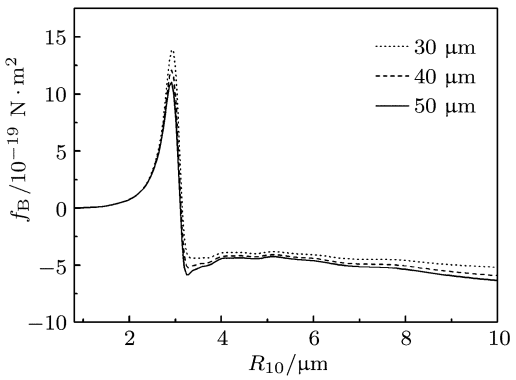


Fig. 5. Secondary radiation force coefficient $f_{\rm B}$ as a function of the radius of the first microbubble.

Figure 6 shows the evolution of the average relative velocity for a selected microbubble pair ($R_{10} = 1.5$ μm, $R_{20} = 2.5$ μm) with an initial distance $D_0 = 40$ μm, where the microbubbles were driven by 2.5 MHz ultrasound with the acoustic pressure of 0.1 MPa. As can be seen, the average relative velocity gradually increases with time, and had a rapid growth after about 1 ms. It indicates that the microbubble attraction accelerates rapidly with the elapsed time. The relative velocities at 1.2 ms at three driving frequencies of 2.25, 2.5 and 3 MHz were 0.86, 9.4, and 0.57 cm/s, respectively. It is found that the velocity at the frequency of 2.5 MHz is much larger than those at other frequencies. Although the frequencies of 2.25 and 2.5 MHz were smaller than both the resonant frequencies of the two microbubbles (5.8 and 2.79 MHz), the frequency of 2.5 MHz was quite close to the resonant frequency of the larger microbubble. As a result, stronger attractive interaction was produced at 2.5 MHz. As the frequency of 3 MHz was between the two resonant frequencies, there was a mild repulsion according to the preceding analysis in Fig. 2. It suggests that the driving frequency lying outside of both resonant frequencies would lead to the attraction of microbubbles; the frequency being close to the one of the resonant frequencies results in more rapid attraction. Otherwise, repulsion occurs if the driving frequency is between the two resonant frequencies. Therefore, it might be desirable to make the mean microbubble radius deviate from the resonance radius to inhibit microbubble aggregation, which can be achieved by controlling the distribution of microbubbles. Note that this study assumes that the space between microbubbles is large enough to ensure that the microbubble oscillation remains spherical, the mutual movement outside the range of time shown in the figure is not considered.

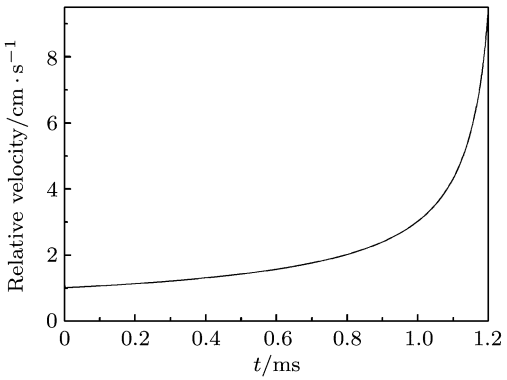


Fig. 6. Evolution of the average attractive relative velocity between the bubble pair $R_{10} = 1.5$ μm, $R_{20} = 2.5$ μm with elapsed time. $P_{\rm a} = 0.1$ MPa, $f = 2.5$ MHz, $D_0 = 40$ μm.

Figure 7 shows the separation distance between the two microbubbles ($R_{10} = 1.5$ μm, $R_{20} = 2.5$ μm) at 106 μs as a function of acoustic pressure for various elastic modulus of the shell. The driving frequency was 2.25 MHz and the initial separation distance was 40 μm. The separation distance between the two microbubbles was found to decrease as the applied acoustic pressure increases. This suggests that increasing the acoustic pressure leads to stronger extent of aggregation of microbubbles. Additionally, for a fixed acoustic pressure, the ability of mutual attraction can be enhanced when the elastic modulus of the shell decreases. Smaller elastic modulus means greater flexibility and stronger ductibility,[25] which also denotes the enhancement of bubble expansion. The coating

material itself carries considerable weight with relative motion between microbubbles. Thus, for the same purpose, low acoustic pressure and contrast agents with small flexibility should be chosen.

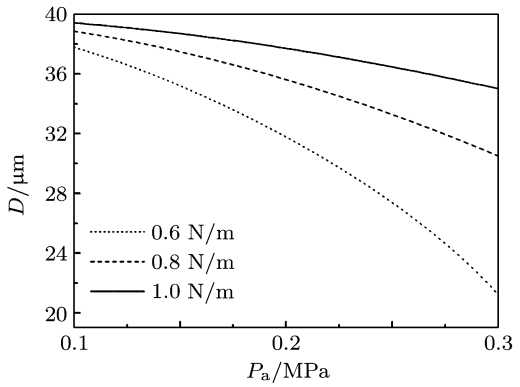


Fig. 7. The separation distance between two microbubbles ($R_{10} = 1.5$ μm, $R_{20} = 2.5$ μm).

4. Conclusion

One major challenge remaining in ultrasonic molecular imaging is the relative low targeting efficiency of contrast agents. One possible reason is the formation of aggregates of microbubbles due to the secondary radiation force between them. This study investigated the influence of the secondary radiation force on microbubble aggregation. Numerical calculations were performed based on the modified Rayleigh-Plesset equation and four simultaneous differential equations of radial and translational motion. The change of secondary radiation force signs and the formation of stable bubble pairs in the vicinity of resonant regions are two important aspects of the dynamic behaviours. Considering the contrast agents used for ultrasound molecular imaging with a size distribution ranging from 0.8 μm to 3 μm, attraction between microbubbles readily occurs in clinical practice, resulting in aggregation of agents. Optimal choices of exciting acoustic parameters (acoustic pressure and driving frequency) and microbubble shell parameters could reduce the possibility of microbubble aggregation. Our findings are important for further developing ultrasound molecular imaging.

References

[1] Winter P M, Caruthers S D, Yu X, Song S K, Chen J J, Miller B, Bulte J W M, Robertson J D, Gaffney P J, Wickline S A and Lanza G M 2003 *Magnetic Resonance in Medicine* **50** 411

[2] Weller G E, Wong M K, Modzelewski R A, Lu E X, Klibanov A L, Wagner W R and Villanueva F S 2003 *Circulation* **108** 515

[3] Zhang C B, Liu Z, Guo X S and Zhang D 2010 *Chin. Phys.* B **20** 024301

[4] Klibanov A, Hughes M, Marsh J, Hall C, Miller J, Wible J and Brandenburger G 1997 *Acta Radiol Suppl.* **412** 113

[5] Lindner J R, Jayaweera A R, Sklenar J and Kaul S 2002 *J. Am. Soc. Echocardiogr* **15** 396

[6] Huang B, Zhang Y L, Zhang D and Gong X F 2010 *Chin. Phys.* B **19** 054302

[7] Li X C and Sun X D 2011 *Chin. Phys.* B **19** 119401

[8] Keller M W, Segal S S, Kaul S and Duling B R 1989 *Circ. Res.* **65** 458

[9] Zhao S, Borden M, Bloch S H, Kruse D, Ferrara K W and Dayton P A 2004 *Mol. Imaging* **3** 135

[10] Hu Y, Ge Y, Zhang D, Gong X F and Zheng H R 2009 *Acta Phys. Sin.* **58** 4746 (in Chinese)

[11] Dayton P A, Morgan K E, Klibanov A L, Brandenburger G, Nightingale K R and Ferrara K W 1997 *IEEE Trans. Ultrason. Ferroelectr. Freq. Control* **44** 1264

[12] Dayton P A, Morgan K E, Klibanov A L, Brandenburger G H and Ferrara K W 1999 *IEEE Trans. Ultrason. Ferroelectr. Freq. Control* **46** 220

[13] Ilinskii Y A, Hamilton M F and Zabolotskaya E A 2007*J. Acoust. Soc. Am.* **121** 786

[14] Naoe T and Futakawa M 2007 *Phys. Rev.* E **76** 046309

[15] Yasui K, Iida Y, Tuziuti T, Kozuka T and Towata A 2008 *Phys. Rev.* E **77** 016609

[16] Ida M 2009 *Phys. Fluids* **21** 113302

[17] Doinikov A A and Zavtrak S T 1995 *Phys. Fluids* **7** 1923

[18] Doinikov A A and Zavtrak S T 1996 *J. Acoust. Soc. Am.* **99** 3849

[19] Akhatov I, Parlitz U and Lauterborn W 1996 *Phys. Rev.* E **54** 4990

[20] Lauterborn W and Ohl C D 1997 *Ultrason. Sonochem.* **4** 65

[21] Mettin R, Akhatov I, Parlitz U, Ohl C D and Lauterborn W 1997 *Phys. Rev.* E **56**, 2924

[22] Doinikov A A 2001 *Phys. Rev.* E **64** 026301

[23] Yasui K, Lee J, Tuziuti T, Towata A, Kozuka T and Iida Y 2009 *J. Acoust. Soc. Am.* **126** 973

[24] Marmottant P, van der Meer S, Emmer M and Versluis M 2005 *J. Acoust. Soc. Am.* **118** 3499

[25] Church C C 1995 *J. Acoust. Soc. Am.* **97** 1510